

“Shadow” Synthesis, Structure, and Electronic Properties of [2.2](1,6)(1,8)Pyrenophane-1-monoene

Kiran Sagar Unikela, Zahra A. Tabasi, Louise N. Dawe, Yuming Zhao, and Graham J. Bodwell*

Cite This: *J. Org. Chem.* 2021, 86, 4405–4412

Read Online

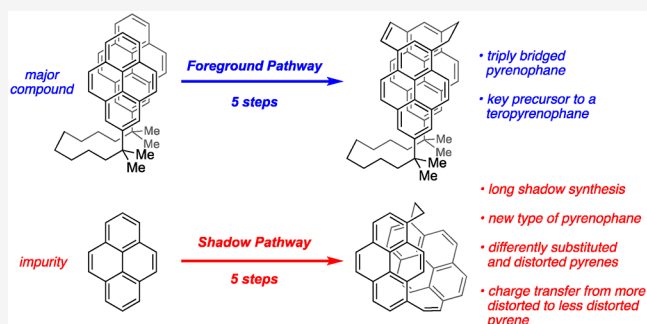
ACCESS |

Metrics & More

Article Recommendations

Supporting Information

ABSTRACT: An unexpected side product of a McMurry reaction was found to be a new [2.2]pyrenophane consisting of two pyrene units with different substitution patterns as well as different types and degrees of distortion from planarity. The new pyrenophane exhibits both monomer and intramolecular excimer fluorescence. Natural bond orbital (NBO) analysis revealed that there is an intramolecular charge-transfer interaction from the more distorted pyrene system to the less distorted one. The origin of the new pyrenophane was traced back to an impurity that was present a full five steps prior to the McMurry reaction from which it was isolated. The pathway to the pyrenophane shadowed that of the main synthetic route.



INTRODUCTION

Organic reactions seldom afford the desired product(s) without the formation of byproducts or side products.¹ Consequently, the separation of the various reaction products is normally required and it is often the most time-consuming part of completing a reaction. Isolating and identifying side products requires effort, but it can provide valuable information about the chemistry at hand and this, in turn, can be used to identify superior reaction conditions, to underpin the development of new reactions or even to spark the pursuit of new research directions.

There are three main sources of side products in an organic reaction: the starting material, the product, and impurities in the starting material. With regard to the starting material, side products originate from unanticipated competing reaction pathways. “Follow-on” side products can form if the intended product is reactive under the conditions of its formation. Finally, the presence of one or more impurities in the starting material can result in the formation of side products that, on first inspection, are very surprising. The formation of side products in this fashion is hardly remarkable, but it is quite uncommon for an impurity to be carried through several steps of a synthetic sequence, while not only undergoing appropriate reactions at every step but also evading separation and/or detection. Rarer still is when such a “shadow” synthesis delivers a compound that is interesting in its own right. We report here the isolation of a product of such a synthesis, a new [2.2]pyrenophane.

The [2.2]cyclophanes, which consist of two aromatic systems and two 2-carbon bridges, are one of the most populous classes of cyclophanes.² They have attracted broad attention because the two aromatic systems are normally held

close to one another in a specific orientation. This enables the study of how the two aromatic systems interact with one another.

For any given pair of aromatic compounds, the relative orientation of the two aromatic systems can be varied by changing their respective bridging motifs. Starting with benzene, only the (1,3) and (1,4) bridging motifs are possible, which means that there are just three constitutionally isomeric [2.2]benzenophanes, 1–3 (Chart 1). (The total of three excludes ortho substituted benzene rings. The inclusion of ortho substituted benzene rings brings the total to six.²¹) As the arenes become larger, more bridging motifs become available and this translates into more ways of orienting the two arenes with respect to one another.³

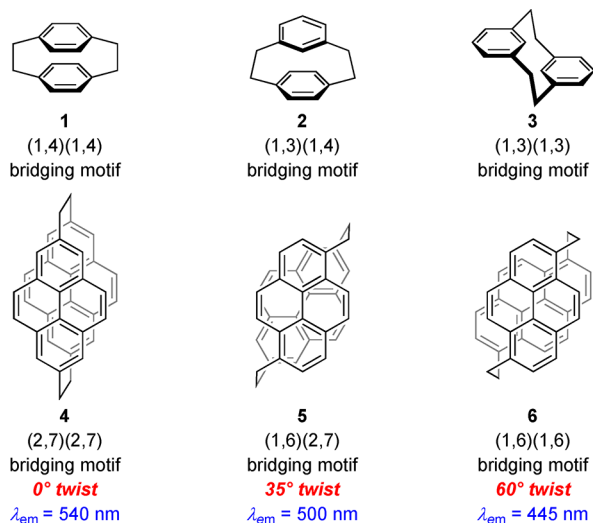
In the case of pyrene, which is of broad interest due to its applications in fluorescent molecules/materials⁴ and fluorescence-based sensing,⁵ there are 12 possible bridging motifs,³ which means that there are 78 possible constitutionally isomeric [2.2]pyrenophanes. (For an arene with n available bridging motifs, the number of possible combinations in a [2.2]cyclophane is described by the triangular number T_n , which is the sum of the integers from 1 to n .) In fact, only five of them have been realized: (1,3)(1,3), (1,6)(1,6), (1,6)(2,7), (1,8)(1,8), and (2,7)(2,7).³ From three of the systems that

Received: October 29, 2020

Published: March 3, 2021



Chart 1. Some Benzene and Pyrene-Based [2.2]Cyclophanes (1–6) with Different Bridging Motifs

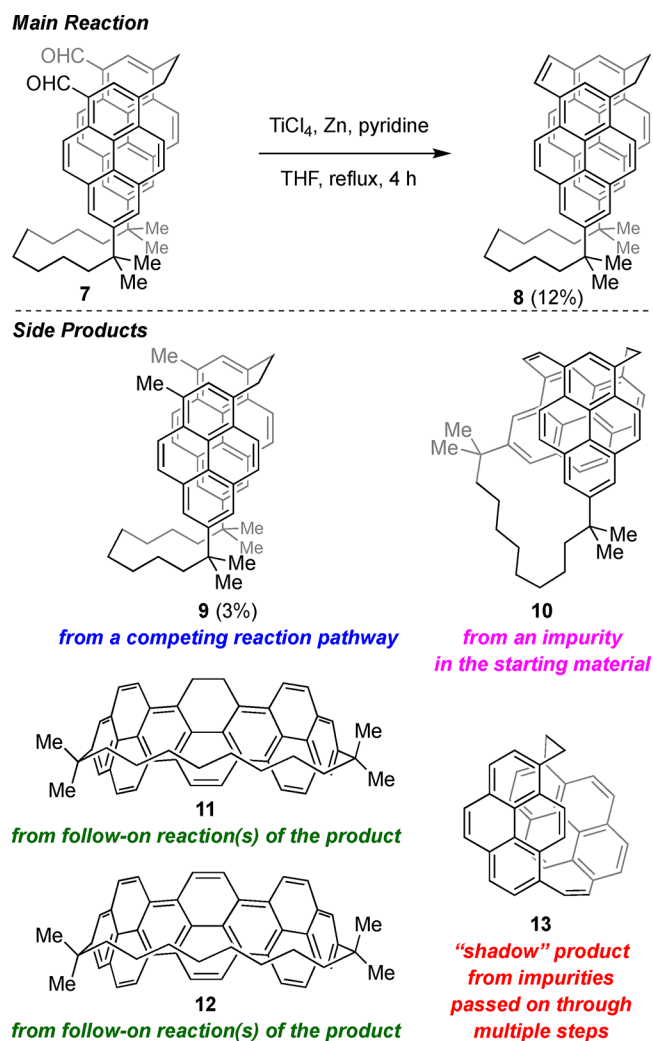


have been synthesized (4–6), it has been learned that excimer formation (a very important characteristic of pyrene, upon which much of its sensing behavior is based) is sensitive to how the two pyrene systems are oriented with respect to one another. The best planes of the two pyrene units in these systems are more or less parallel, but twisted to varying amounts with respect to an orthogonal axis. The 0° twist in pyrenophane **4** appears to be best for excimer emission.⁶ This compound exhibits a strong emission band centered at 540 nm. Pyrenophane **5**,⁷ which has a 35° twist, also exhibits excimer emission, but it is weaker and at higher energy (500 nm). Moving to pyrenophane **6** (60° twist),⁷ the emission is again more intense, but is now observed at 440–450 nm, which is typical of monomer emission. Although the pyrenophanes 4–6 have revealed how the relative positioning of two pyrene systems can have a strong influence on the emission behavior, a deeper understanding of this phenomenon will require access to more than just three compounds.

RESULTS AND DISCUSSION

We recently reported the synthesis of 1,1,10,10-tetramethyl-[10](2,11)teropyrenophane (**12**) as part of a study aimed at the development of a general gram-scale synthesis of the 1,1,*n,n*-tetramethyl[*n*](2,11)teropyrenophanes.^{8a} One of the key C–C bond-forming steps was the intramolecular McMurry reaction of [10.2](7,1)pyrenophanedialdehyde **7** to afford triply bridged [10.2.2](7,1,3)pyrenophane **8** (Scheme 1). In contrast to the analogous reactions of the next three lower homologues, the reaction of dialdehyde **7** gave a cluster of products with very similar R_f values. The desired pyrenophane **8** was isolated in pure form only after extensive chromatography (at least 15 columns) to separate it from five closely eluting side products. (The large-scale synthesis of teropyrenophane **12**, which was the most problematic one of the series,^{8a} was performed on only one occasion.) Interestingly, the set of side products exemplifies the different ways in which side products can arise. Dimethylpyrenophane **9** comes from a competing reaction pathway (reduction of the formyl groups in **7** instead of reductive coupling). Cyclophane-monoene **10** is the product of an intramolecular McMurry reaction of a regioisomer of **7**, which must have been present as an impurity.

Scheme 1. Compounds Isolated from the Intramolecular McMurry Reaction of [10.2]Pyrenophanedialdehyde **7**



Dihydroteropyrenophane **11** arises from closure of the central C–C bond in **8** under the conditions of its formation, and teropyrenophane **12** is the product of dehydrogenation of **11**. The formation of both of these follow-on side products is noteworthy in that they did not occur for the lower homologues in the series (where the long bridge is 7–9 atoms in length) and that formal oxidation reactions (dehydrogenations) took place under reductive conditions.

Identification of the final side product was less straightforward. APCI(+)-LC-MS analysis showed a strong peak at $m/z = 455$, which corresponds to $[M + H]^+$ of a [2.2]pyrenophanemonoene ($\text{C}_{36}\text{H}_{22}$) without a long bridge. The absence of high-field aliphatic signals in the ^1H and ^{13}C NMR spectra supported this conclusion. In the ^{13}C NMR spectrum, 34 signals in the range δ 119–136 ppm were observed, which is consistent with the presence of two pyrene systems with different substitution patterns ($2 \times 16\text{C}$) and an alkene (2C). The aliphatic region showed just two signals for a saturated 2C (ethano) bridge. This ruled out dealkylation of **8**. Dealkylation of **10** was also ruled out by the absence of any ABC spin systems in the aromatic region of the ^1H NMR spectrum, which spanned a very broad chemical shift range (δ 8.3–4.6) (see below). Further analysis of the ^1H NMR spectrum pointed toward (1,6) and (1,8) substitution patterns for the

two pyrene systems, which left [2.2](1,6)(1.8)pyrenophane-1-monoene **13** as the only possible structure (Supporting Information). COSY and NOESY experiments were then used to assign most of the protons, which were very close to calculated values (GIAO/B3LYP/6-311+G(2d,p) level of theory, Supporting Information). The structure was then unambiguously determined using X-ray single crystal diffraction (XRD) analysis (Figure 1). The origin of this side product is discussed in detail below.

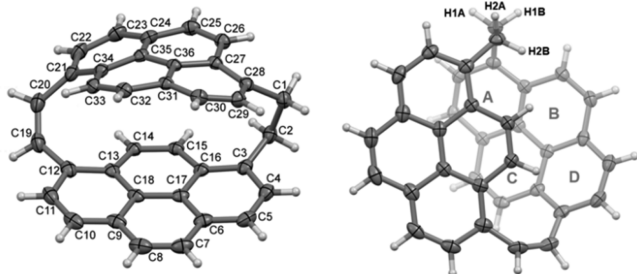


Figure 1. Two views of pyrenophane **13** from the crystal structure, represented with 50% probability ellipsoids. Crystallographic numbering is shown. CCDC 2034879.

In the crystal, the 1,8-disubstituted ring of **13** is bent out of planarity, but only marginally (Figure 1). The bend angle θ (the smallest angle formed between the planes defined by atoms [C3, C4, C16] and atoms [C11, C12, C13]) is just 9.7° . This value is substantially smaller than that of the pyrene unit in 1,12-dioxo[12](2,7)pyrenophane ($\theta = 34.6^\circ$),¹⁰ which houses the least bent pyrene system of any reported [*n*](2,7)pyrenophane. More substantial distortion from planarity is present in the 1,6-disubstituted pyrene system. In this case, the (1,6) bridging motif causes a longitudinal twist and a diagonal bend. The diagonal bend can be quantified using an angle analogous to θ . Like θ , each plane is defined by a set of three atoms, which includes the bridgehead carbon atom and the two flanking atoms in the pyrene system to which it is bonded. To differentiate these angles, they can be referred to as $\theta_{2,7}$ and $\theta_{1,6}$. Thus, the angle $\theta_{1,6}$ in **13** is the smallest angle formed between the planes containing atoms [C21, C22, C34] and atoms [C27, C28, C29] and its value is 44.0° . This is substantially larger than the corresponding values in [10](1,6)pyrenophane (**14**) (27.3°)¹¹ and the more elaborate (1,6)pyrenophane **15** (17.4°)¹² (Chart 2).

Pyrenophane **13** is chiral by virtue of the (1,6) bridging motif in one of the pyrene systems. The space group (*C2/c*) is centrosymmetric. Adjacent molecules in the packed unit cell

have opposite configurations (Figure S3), and close supramolecular C–H $\cdots\pi$ interactions between neighboring molecules lead to a chain-like arrangement (Figures S5, S6) with H-to-centroid distances ranging from 2.74 to 3.04 Å (Table S1).

The degree of twist can be quantified by examining the dihedral angles along the benzylic-to-benzylic pathway through the center of the pyrene system (Table S2). Increasing deviation of these angles from 180° is a reflection of increasing twist in the pyrene system. For **13**, the dihedral angles along the [C20, C21, C34, C35, C36, C27, C28, C1] pathway are -153.0° , 159.0° , -158.9° , 159.7° , and -150.7° . The deviation from 180° ranges from 20.3° to 29.3° , and the average value is 23.8° . By comparison, the deviation from 180° in [10](1,6)pyrenophane (**14**) spans a range of 9.5° to 20.1° and has an average value of 14.1° . In **15**, the range is 5.9° to 20.0° and the average is 10.8° . Alternatively, two twisted naphthalene units (rings AB and rings CD) can be identified within the 1,6-disubstituted pyrene system and their twist angles can be considered.¹³ The twist angles for the AB and CD naphthalene systems are 16.9° and 18.2° , respectively. Thus, the degree of twist is significant. The naphthalene twist angles for **14** and **15** were not reported, but have now been determined using the original data to be substantially lower than those in **13** (9.7° and 9.5° for **14**; 7.5° and 4.3° for **15**). On the other hand, the values for **13** are well short of those observed in more highly strained systems such as 1,7-dioxo[7](2,7)pyrenophane (**16**, 37°)¹⁴ and [2](6,1)naphthaleno[1]paracyclophane (**17**, 35.1°)¹⁵ both of which required powerful aromatization-based methods for their synthesis.

The slipped stacking arrangement of the two pyrene systems in **13** means that one edge of each of the pyrene systems lies over the face of the other (Figure 1, right). Consequently, these protons are observed at unusually high field in the ^1H NMR spectrum (Figure 2). The highest field signals are

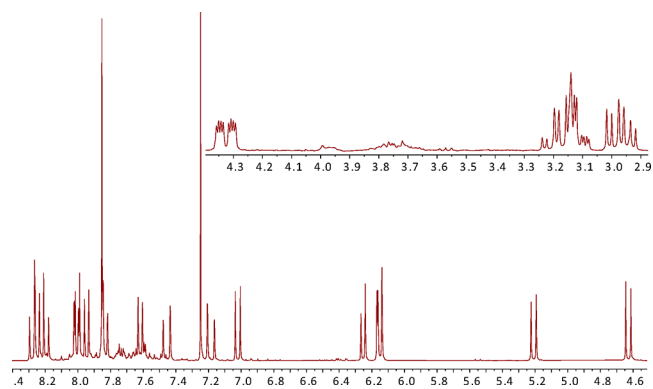
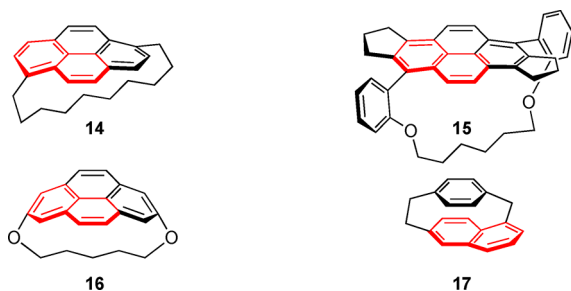


Figure 2. Aromatic and aliphatic regions of the 300 MHz ^1H NMR spectrum of pyrenophane **13** in CDCl_3 .

Chart 2. Comparison Compounds 14–17^a



^aA twisted naphthalene unit in each molecule is colored red.

observed for the protons attached to the *K*-region located between the two bridgeheads of the 1,8-disubstituted pyrene system, which appear as an AX system at δ 5.22 and 4.64 ppm ($J = 9.5$ Hz). The shielded edge of the 1,6-disubstituted pyrene appears as an AX system at δ 7.03 and 6.17 ppm ($J = 9.0$ Hz) for the *K*-region and another AB system δ 6.26 and 6.16 ppm ($J = 7.7$ Hz). The alkene protons are observed as an AB system at δ 7.45 and 7.18 ppm with an unusually large coupling constant for a *Z*-configured alkene ($J = 13.2$ Hz). This large value may be related to some combination of the rather low dihedral angles between the alkene and the two pyrene systems

to which it is attached (deviation from $90^\circ = 37.9^\circ\text{--}49.0^\circ$), or the very large C=C bond angles of the alkene bridge (134.2° and 128.7°). Four signals are observed for the aliphatic bridge protons, which indicates that there is no interconversion between enantiomers via ring flipping at room temperature. Simple inspection of molecular models suggests that this would be an exceedingly high energy process. The bridge proton H_{1b} (Figure 1, right) resonates at much lower field (δ 4.32 ppm) than the other three (H_{1a} at δ 2.97 ppm, H_{2a} at δ 3.12 ppm, H_{2b} at δ 3.18 ppm). The low field shift is presumably due to steric deshielding arising from its close contact ($2.12(2)$ Å) to the *peri*-proton C29(H) (NOE cross peak). The proton H_{2b} has a similar *peri*-contact to C15(H) ($2.18(2)$ Å), but the steric deshielding here appears to be counteracted by shielding from the opposite pyrene system. Examination of the *gauche* coupling constants within the aliphatic bridge ($J(H_{1a}\text{--}H_{2a}) = 5.3$ Hz, $J(H_{1b}\text{--}H_{2a}) = 2.3$ Hz, $J(H_{1b}\text{--}H_{2b}) = 4.7$ Hz, Supporting Information) suggests that the solution structure of **13** is close to the crystal structure. In the crystal structure, the C28–C1–C2–C3 dihedral angle (51.5°) reveals a small deviation from perfect staggering, which means that the $H_{1b}\text{--}C\text{--}C\text{--}H_{2a}$ dihedral angle should be closer to 90° than the other *gauche* relationships and $J(H_{1b}\text{--}H_{2a})$ should therefore be the smallest.

The absorption spectrum of **13** in chloroform shows a long-wavelength absorption tail ranging from 390 to 550 nm, along with three significant absorption bands at 358, 343, and 278 nm (Figure 3). According to TD-DFT calculations (Table S4),

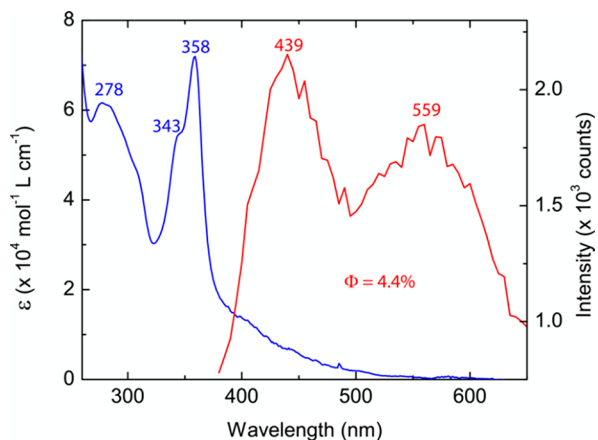


Figure 3. UV–vis absorption (blue trace) and fluorescence (red trace, $\lambda_{\text{exc}} = 345$ nm) spectra of pyrenophane **13** measured in chloroform.

the low-energy absorption bands in the UV–vis spectrum of **13** are mainly due to the electronic transitions among the frontier molecular orbitals of **13**. The experimentally observed long-wavelength absorption tail matches the calculated HOMO to LUMO transition at 420 nm, while the intense absorption bands at 358 and 343 nm in the UV–vis spectrum agree well with the TD-DFT calculated HOMO–1 to LUMO and HOMO to LUMO+1 transitions, respectively (Figure 4).

The fluorescence spectrum of pyrenophane **13** shows two emission bands at 439 and 559 nm. The first emission band (439 nm) can be assigned as the S_1 to S_0 transition. Due to the difficulty in determining the exact λ_{max} value for the long-wavelength absorption tail in the UV–vis absorption spectrum, the Stokes shift of **13** cannot be precisely calculated. Nevertheless, the significant spectral overlap between the

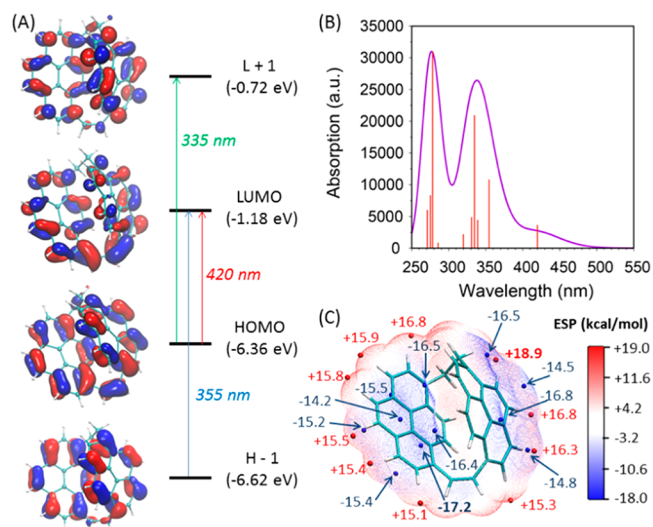


Figure 4. (A) Contours (isovalue = 0.03 au) and eigenvalues (in eV) of the frontier molecular orbitals for pyrenophane **13**. TD-DFT calculated absorption wavelengths are indicated. (B) TD-DFT simulated UV–vis absorption spectrum of **13**. (C) Molecular electrostatic potential map of **13** with maximum and minimum potential points (kcal/mol) indicated. All calculations performed at the CAM-B3LYP/6-311+G(2d,p)//B3LYP/6-31G(d) level of theory.

long-wavelength UV–vis absorption tail and the first emission band in the fluorescence spectrum suggests a small Stokes shift and hence a high degree of structural similarity between the first excited state (S_1) and the ground state (S_0). This outcome is consistent with the apparent structural rigidity of cyclophane **13**. The long-wavelength emission band at 559 nm appears to be broader and weaker than the first emission band at 439 nm. This band can be reasonably attributed to the characteristic emission of the pyrene excimer.¹⁶ Since lowering the concentration of **13** (from 10^{-5} to 10^{-6} M) did not result in significant attenuation of this band, the pyrene excimer is likely formed intramolecularly given the close distance and partial ring overlap between the two pyrene units in the structure of **13**. The relative fluorescence quantum yield (Φ_F) of **13** was determined to be 4.4% in chloroform. It is possible that the significant intramolecular interactions between the two pyrene units in **13** (see below) facilitate nonradiative decay, which in turn result in a low degree of emission efficiency. The excitation spectra monitored at 470 and 550 nm (Figure S10) support the notion that both emission bands are intrinsic to the molecule, but also point toward more complex behavior in the excitation manifold. More detailed study of this behavior is warranted.

The electrostatic potential map of **13** reveals that both of the pyrene systems bear a greater accumulation of π -electron density on the outer surface than on the inner surface (Figures 4C, S7). This is presumably due to electronic repulsions between the inner surfaces of the two π systems where they are held close to one another. The largest negative potential point on the outer face of the 1,8-disubstituted pyrene unit has a larger value (-17.2 kcal/mol) than that of the outer face of the 1,6-disubstituted pyrene unit (-16.8 kcal/mol). The two pyrene systems also feature outer edges with larger positive potentials than their inner edges, but it is now the 1,6-disubstituted pyrene unit that has the greater largest positive potential point ($+18.9$ kcal/mol vs $+16.8$ kcal/mol). The combination of negatively charged outer surfaces and positively

charged outer edges likely promotes the prominent edge-to-face interactions observed in the crystal structure (Figure S5). Interestingly, in the crystal, the outer edges of each type of pyrene unit interact only with outer surfaces of the same type, i.e. (1,6) with (1,6), and (1,8) with (1,8).

Using NBO analysis, three distinct through-space interactions between a π bonding orbital located on the more distorted 1,6-disubstituted pyrene unit with a π^* antibonding orbital on the less distorted 1,8-disubstituted pyrene were identified (Figure 5). The total delocalization energy ($E(2)$)

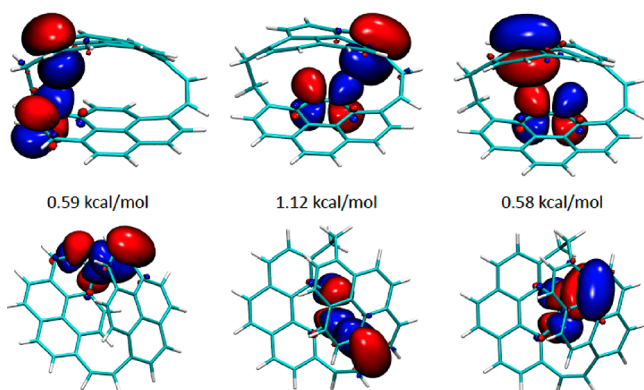


Figure 5. Plots of natural bond orbitals (isovalue = 0.03 au) showing three donor–acceptor orbital interactions between the two pyrene units in pyrenophane **13**. Top: viewed from the side, and bottom: viewed from the top. Calculated at the M06-2X/Def2SVP//B3LYP/6-31G(d) level of theory.

arising from these donor–acceptor orbital interactions was calculated to be 2.29 kcal/mol. In addition to the through-space orbital interactions between the two pyrene units, the 1,6-disubstituted pyrene was found to contribute a π orbital interacting with the $\pi_{C=C}^*$ antibonding orbital of the alkene bridge ($E(2) = 8.32$ kcal/mol), while a π orbital of the 1,8-disubstituted pyrene shows hyperconjugative interaction with the σ_{C-C}^* of the ethano bridge ($E(2) = 3.14$ kcal/mol) (Figure S8). Overall, the orbital interactions suggest the occurrence of charge transfer from the 1,6-disubstituted pyrene system to the 1,8-disubstituted pyrene system, which may explain the differences in electrostatic potential between the outer surfaces and outer edges of the two pyrene systems.

To further examine the charge transfer properties in pyrenophane **13**, natural population analysis (NPA) was carried out. The 1,6-disubstituted pyrene unit possesses a total NBO charge of +0.07, while the 1,8-disubstituted pyrene unit shows a total NBO charge of -0.037 . The different amounts of charge distributed on the two pyrenyl groups also point to a mild degree of charge transfer from the bent and twisted 1,6-disubstituted pyrene system to the relatively flat 1,8-disubstituted one.

Dipole moment analysis also supported the existence of intramolecular charge transfer. The net molecular dipole moment of **13** was calculated to be 1.094 D, and its direction coincides with the alignment of donor-to-acceptor bonds shown in the NBO analysis (Figure 6). The 1,6-disubstituted pyrene contributes a dipole moment of 0.263 D, which is roughly perpendicular to its best plane and points toward the 1,8-disubstituted pyrene system beneath it. The 1,8-disubstituted pyrene unit contributes a dipole moment of 1.001 D. The vector of this dipole is on the pyrene surface and

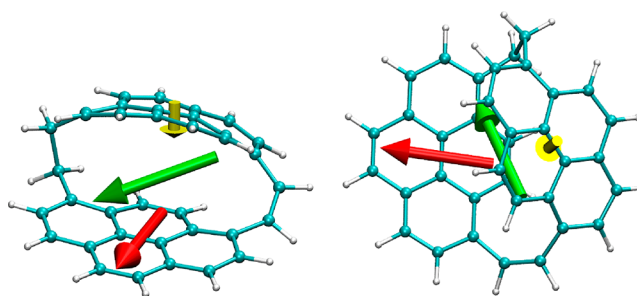


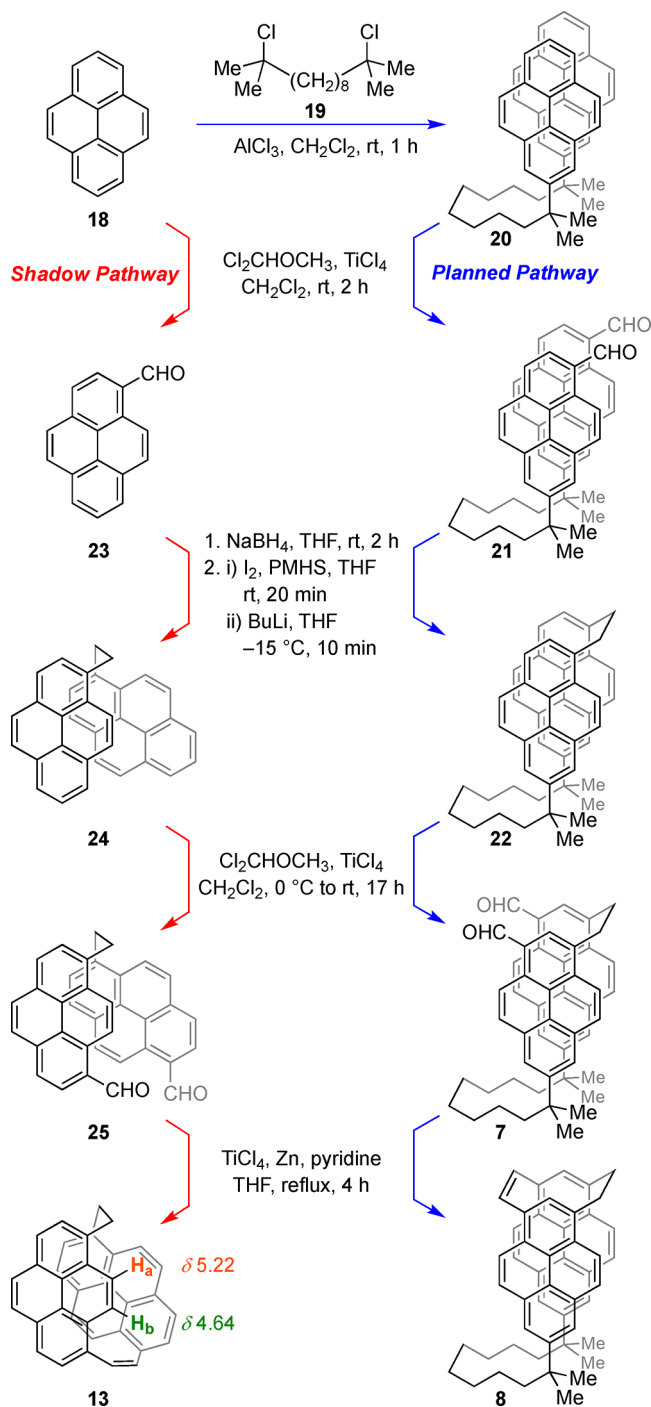
Figure 6. Dipole moments contributed from the entire molecule (green arrow), 1,6-disubstituted pyrene (yellow arrow), and 1,8-disubstituted pyrene (red arrow). Left: viewed from the side, and right: viewed from the top. Calculated at the M06-2X/Def2SVP//B3LYP/6-31G(d) level of theory.

perpendicular to the nodal direction (2,7-positions). The molecular dipole includes contributions from the two bridges in addition to those from the two pyrene systems.

With regard to the origin of [2.2]pyrenophane **13**, it can be traced back to the synthesis of dipyren-2-ylalkane **20**, which was accomplished *via* a Friedel–Crafts alkylation reaction of pyrene (**18**) using dichloride **19** (Scheme 2). The reaction was performed using dichloride **19** and a 10-fold excess of pyrene (**18**, 219 g) to suppress the formation of linear oligomers. The desired product **20** (54%) was separated from roughly 196 g of unreacted pyrene using column chromatography. A small amount of pyrene in the sample of **20** is what appears to have served as a starting material for the synthesis of **13** via a route that shadowed the five-step sequence of reactions leading from **20** to cyclophane-monoene **8** (via dialdehyde **21**, [10.2]-cyclophane **22** and dialdehyde **7**).

In the “shadow” synthesis, (Although the concept is surely not new, we suggest the name “shadow synthesis” and the following definition: a shadow synthesis is one in which an impurity in a starting material or synthetic intermediate in a synthetic sequence is carried through more than one step of that sequence while undergoing appropriate chemistry at every stage and evading separation until it is isolated.) Rieche formylation of pyrene (**18**) presumably afforded pyrene-1-carboxaldehyde **23**.¹⁷ Reduction would then have led to 1-(hydroxymethyl)pyrene, self-reaction of which in the subsequent iodination / Wurtz coupling protocol would have furnished 1,2-dipyren-1-ylethane (**24**). Considering that this compound is the homocoupling product of a minor component of a mixture, it is counterintuitive that any of this compound should form. The implied success of the Wurtz coupling leading to **24** may be a consequence of it being an intermolecular reaction, while the one leading to **22** is intramolecular. If the rate of the intramolecular reaction was substantially faster than any competing intermolecular reactions (including crossed Wurtz couplings), then the major component of the reaction mixture would have been quickly depleted, thereby providing a more favourable environment for the homocoupling of the minor component leading to **24**. Rieche formylation of **24** could conceivably give several dialdehydes arising from reaction at the 3, 6 and 8 positions of the two pyrene systems. 1-Substituted pyrenes are known to undergo electrophilic aromatic substitution reactions preferentially at the 6 and 8 positions, with a slight preference for the 6 position.¹⁸ Thus, at any point up to a 2:1 preference for the 6 position, the most abundant dialdehyde arising from **24** would be **25**. (If the relative rates of reaction of the 6 and 8

Scheme 2. A Portion of the Planned Synthetic Pathway En Route to Teropyrenophane **12** and the Shadow Route from Pyrene (**18**) to Pyrenophane **13**



position are 1:1, the distribution of the (1,6)(1,6), (1,6)(1,8) and (1,8)(1,8) products is 1:2:1. If the relative rates of reaction of the 6 and 8 position are 2:1, the distribution of the (1,6)(1,6), (1,6)(1,8) and (1,8)(1,8) products is 44.4:44.4:11.1.) Intramolecular McMurry reaction of **25** leads directly to **13**.

Perhaps the most noteworthy features of the shadow synthesis of **13** is the number of steps (five) through which synthetic intermediates were not detected or separated (including chromatographic purifications of **21**, **22**, and **7**).

(Small peaks corresponding to pyrene (**18**), pyrene-1-carbaldehyde (**23**), and 1-(hydroxymethyl)pyrene (not shown) were observed in the LCMS and HRMS spectra of **20**, **21** and its reduction product (not shown), respectively. These signals are most likely due to the presumed impurities, but could also arise from retro-Friedel–Crafts *t*-alkylation of the main compounds in the instrument.) To date, we have not found any other example of a shadow synthesis of this length. The success of the McMurry reaction in generating **13** is also interesting because this methodology has a long track record of performing poorly in the synthesis of [2.2]cyclophanes that have even a moderate amount of strain.^{18,19} In this regard, it is noteworthy that the orbital interactions discussed above offer a significant degree of stabilization to the structure of pyrenophane **13** and this stabilization may have contributed to the success of this particular McMurry reaction. The calculated (M06-2X/Def2SVP//B3LYP/6-31G(d)) strain energy of **13** is 14.4 kcal/mol (Supporting Information). (The value calculated at the B3LYP/6-31g(d) level of theory (21.1 kcal/mol) is 47% higher. The use of the M06-2X functional includes dispersion, so it gives more reliable values for strain energies.²²) The clear implication is that analogous reactions leading to [2.2]pyrenophanes with other new bridging motifs may also fare well. Furthermore, the synthetic strategy of using a Wurtz coupling to form the first bridge and then an intramolecular McMurry reaction to form the second might prove to be generally applicable to [2.2]cyclophanes with aromatic systems larger than benzene. To test this, the first action would be to intentionally synthesize **13** using the shadow pathway. This could be followed by work aimed at the synthesis of other [2.2]pyrenophanes and/or PAH-based [2.2]cyclophanes.

CONCLUSION

The isolation of pyrenophane **13** from the McMurry reaction of dialdehyde **7** was surprising because it could not possibly have originated from the starting material or any of the possible side products arising from the previous reaction. Its genesis was eventually traced back to an impurity that was present at a much earlier stage in the synthetic sequence. This impurity (pyrene) must have been carried through five synthetic steps and not only have undergone appropriate chemistry that shadowed the chemistry of the major compound but also evaded separation. The success of the shadow synthesis suggests that the Wurtz coupling/intramolecular McMurry strategy may be more widely applicable to the synthesis of PAH-based [2.2]cyclophanes. The two differently substituted pyrene systems in **13** are distorted in different ways and to quite different extents. The 1,8-disubstituted pyrene is very gently bent out of planarity, while the 1,6-disubstituted pyrene is bent and twisted to a greater extent than in all previously reported (1,6)-pyrenophanes. Pyrenophane **13** was found to exhibit dual monomer/excimer emission, albeit relatively weak. More significantly, NBO analysis, NPA, and dipole moment analysis all pointed toward the presence of intramolecular charge-transfer interactions between the bent and twisted 1,6-disubstituted pyrene unit and the nearly planar 1,8-disubstituted pyrene unit. This raises the intriguing possibility that distortion from planarity might prove to be a means to induce charge transfer between two otherwise electronically similar π systems. Further investigation of this issue is warranted. Finally, the differences in electron density between

the two edges of each pyrene system suggests that **13** may exhibit unusual regioselectivity in its electrophilic aromatic substitution chemistry.

EXPERIMENTAL SECTION

General. ^1H , ^{13}C , and 2-D NMR spectra were recorded using CDCl_3 solutions at 300 MHz (75 MHz for ^{13}C) on a Bruker AVANCE III multinuclear spectrometer with a BBFO probe. All NMR spectra are referenced to Me_4Si ($\delta_{\text{H}} = 0.00$ ppm) and CDCl_3 ($\delta_{\text{H}} = 7.26$ ppm). Structural assignments were made with additional information from gCOSY and gNOESY experiments. LCMS data were obtained using an Agilent 1100 series LC/MSD instrument, and high resolution mass spectroscopic data were obtained using an Agilent 6200 series Accurate-Mass-Time-of-Flight instrument. UV-vis absorption analysis was conducted on a Cary 6000i spectrophotometer. A sample of **13** was dissolved in chloroform and measured with a 1 cm quartz cuvette at room temperature. Fluorescence spectra were measured on a Photon Technology International (PTI) QuantaMaster spectrofluorometer. The relative fluorescence quantum yield (Φ_{F}) was measured following reported procedures,²⁰ with quinine sulfate ($\Phi_{\text{F}} = 0.546$) as the standard. Single crystal X-ray data were collected on a Bruker Apex II Diffractometer equipped with an Apex II CCD detector, using Mo X-ray radiation. Crystals of **13** were obtained from slow evaporation of a dichloromethane/hexanes solution.

Cyclophane **13**^{8a} (5 mg) was obtained as a brown solid: $R_{\text{f}} = 0.36$ (10% dichloromethane/hexanes); ^1H NMR (300 MHz, CDCl_3) δ 8.29 (d, $J = 9.2$ Hz, 1H), 8.26 (d, $J = 7.9$ Hz, 1H), 8.20 (d, $J = 9.1$ Hz, 1H), 8.02 (dd, $J = 7.9, 0.6$ Hz, 1H), 8.01 (d, $J = 8.0$ Hz, 1H), 7.96 (d, $J = 7.9$ Hz, 1H), 7.86 (s, 2H), 7.84 (dd, $J = 8.0, 0.6$ Hz, 1H), 7.63 (d, $J = 7.9$ Hz, 1H), 7.47 (d, $J = 13.2$ Hz, 1H), 7.20 (d, $J = 13.2$ Hz, 1H), 7.03 (d, $J = 9.0$ Hz, 1H), 6.26 (d, $J = 7.7$ Hz, 1H), 6.17 (d, $J = 9.2$ Hz, 1H), 6.16 (d, $J = 7.3$ Hz, 1H), 5.22 (d, $J = 9.5$ Hz, 1H), 4.64 (d, $J = 9.5$ Hz, 1H), 4.32 (ddd, $J = 12.7, 4.6, 2.3$ Hz, 1H), 3.18 (ddd, $J = 12.4, 12.4, 4.7$ Hz, 1H), 3.12 (ddd, $J = 12.7, 5.2, 2.2$ Hz, 1H), 2.98 (ddd, $J = 12.3, 12.3, 5.3$ Hz, 1H); $^{13}\text{C}\{^1\text{H}\}$ NMR (75 MHz, CDCl_3) δ 135.0, 134.2, 133.0, 132.1, 130.8, 130.1, 129.3, 129.1, 128.9, 128.8, 128.5, 128.3, 128.2, 128.0, 127.7, 127.2, 127.0, 126.8, 126.6, 126.2, 126.2, 125.9, 125.2, 125.0, 124.9, 124.5, 124.2, 124.2, 124.0, 123.6, 122.0, 121.7, 119.6, 37.6, 31.6; LCMS (CI(+)) m/z (rel. int.) 457 (6), 456 (42), 455 ($[\text{M} + \text{H}]^+$, 100); HRMS (APPI) m/z $[\text{M} + \text{H}]^+$ calcd for $\text{C}_{36}\text{H}_{23}$ 455.1782; found 455.1851.

A yield for **13** (and the other side product **10**) could not be calculated because the mass of its presumed direct synthetic precursor **25** in the sample of **7** was not determined. For context, 3.01 g of dialdehyde **7** were used in the McMurry reaction from which **13** was isolated. Following extensive chromatography, 320 mg (12%) of the desired product **8** were obtained along with 80 mg (3%) of the reduced product **9**, 74 mg of the side product **10**, 55 mg (2%) of the follow-on product **11**, and 3 mg of the follow-on product **12** (0.1%). Thus, the amount of **13** (5 mg) obtained most closely resembles that of **12**.

ASSOCIATED CONTENT

Supporting Information

The Supporting Information is available free of charge at <https://pubs.acs.org/doi/10.1021/acs.joc.0c02579>.

Characterization data, 1-D and 2-D NMR spectra and explanation of proton assignments for **13**, and additional crystallographic information for **13**; details of UV-vis spectroscopy, fluorescence spectroscopy, and computational work; excitation spectra (PDF)

Accession Codes

CCDC 2034879 contains the supplementary crystallographic data for this paper. These data can be obtained free of charge via www.ccdc.cam.ac.uk/data_request/cif, or by emailing data_request@ccdc.cam.ac.uk, or by contacting The Cam-

bridge Crystallographic Data Centre, 12 Union Road, Cambridge CB2 1EZ, UK; fax: +44 1223 336033.

AUTHOR INFORMATION

Corresponding Author

Graham J. Bodwell – Department of Chemistry, Memorial University of Newfoundland, St. John's, NL, Canada A1B 3X7; orcid.org/0000-0002-9476-2078; Phone: +1-709-864-8406; Email: gbodwell@mun.ca

Authors

Kiran Sagar Unikela – Department of Chemistry, Memorial University of Newfoundland, St. John's, NL, Canada A1B 3X7

Zahra A. Tabasi – Department of Chemistry, Memorial University of Newfoundland, St. John's, NL, Canada A1B 3X7

Louise N. Dawe – Department of Chemistry and Biochemistry, Wilfrid Laurier University, Waterloo, ON, Canada N2L 3C5; orcid.org/0000-0003-3630-990X

Yuming Zhao – Department of Chemistry, Memorial University of Newfoundland, St. John's, NL, Canada A1B 3X7; orcid.org/0000-0002-1300-9309

Complete contact information is available at: <https://pubs.acs.org/10.1021/acs.joc.0c02579>

Notes

The authors declare no competing financial interest.

ACKNOWLEDGMENTS

Financial support of this work from the Natural Sciences and Engineering Research Council (NSERC) of Canada is gratefully acknowledged (G.J.B., Y.Z, L.N.D.).

REFERENCES

- (1) Watson, W. On Byproducts and Side Products. *Org. Process Res. Dev.* **2012**, *16*, 1877.
- (2) (a) For the most recent collection of reviews on cyclophanes, see: Special Issue on Cyclophanes, *Isr. J. Chem.* **2012**, *52*(1–2), 1–192. (b) Hassan, Z.; Spuling, E.; Knoll, D. M.; Lahann, J.; Bräse, S. Planar Chiral [2.2]paracyclophanes: From Synthetic Curiosity to Applications in Asymmetric Synthesis and Materials. *Chem. Soc. Rev.* **2018**, *47*, 6947–6963. See also: (c) Hassan, Z.; Spuling, E.; Knoll, D. M.; Bräse, S. Regioselective Functionalization of [2.2]-paracyclophanes: Recent Synthetic Progress and Perspectives. *Angew. Chem., Int. Ed.* **2020**, *59*, 2156–2170. (d) For the most recent book on cyclophanes, see: Gleiter, R.; Hopf, H. *Modern Cyclophane Chemistry*; Wiley: New York, 2004. See also: Keehn, P. M.; Rosenfeld, S. M. *Cyclophanes*; Academic Press: New York, 1983; Vols. 1 and 2. (f) Diederich, F. *Cyclophanes*; The Royal Society of Chemistry: London, 1991. (g) Vögtle, F. *Cyclophane Chemistry*; Wiley: New York, 1983.
- (3) Ghasemabadi, P. G.; Yao, T.; Bodwell, G. J. Cyclophanes Containing Large Polycyclic Aromatic Hydrocarbons. *Chem. Soc. Rev.* **2015**, *44*, 6494–6518.
- (4) (a) Figueira-Duarte, T. M.; Müllen, K. Pyrene-Based Materials for Organic Electronics. *Chem. Rev.* **2011**, *111*, 7260–7314. (b) Casas-Solvas, J. M.; Howgego, J. G.; Davis, A. P. Synthesis of Substituted Pyrenes by Indirect Methods. *Org. Biomol. Chem.* **2014**, *12*, 212–232.
- (5) Vullev, V. I.; Jiang, H.; Jones, G. In *Advanced Concepts in Fluorescence Sensing. Topics in Fluorescence Spectroscopy*; Geddes, C. D., Lakowicz, J. R., Eds.; Springer: Boston, MA, 2005; Vol. 10.
- (6) (a) Irgartinger, H.; Kirrstetter, R. G. H.; Krieger, C.; Rodewald, H.; Staab, H. A. Synthese und Struktur von [2.2][2.7]Pyrenophan.

- Tetrahedron Lett.* **1977**, *18*, 1425–1428. (b) Mitchell, R. H.; Carruthers, R. J.; Zwinkels, J. C. Straining Strained Molecules - I. The Synthesis of the First Cyclophane Within a Cyclophane - [2.2]Paracyclo([2.2]metacyclophane). *Tetrahedron Lett.* **1976**, *17*, 2585–2588. (c) Umemoto, T.; Satani, S.; Sakata, Y.; Misumi, S. Layered Compounds. XXIX. [2.2](2,7)Pyrenophane and its 1,13-Diene. *Tetrahedron Lett.* **1975**, *16*, 3159–3162.
- (7) Kawashima, T.; Otsubo, T.; Sakata, Y.; Misumi, S. Synthesis of Three [2.2]Pyrenophanes as an Excimer Model. *Tetrahedron Lett.* **1978**, *19*, 5115–5118.
- (8) (a) Unikela, K. S.; Ghasemabadi, P. G.; Houska, V.; Dawe, L.; Zhao, Y.; Bodwell, G. J. Gram-Scale Synthesis of the 1,1,*n*-Tetramethyl[*n*](2,11)teropyrenophanes. *Chem. - Eur. J.* **2021**, *27*, 390–400. (b) Unikela, K. S.; Roemmele, T. L.; Houska, V.; McGrath, K. E.; Tobin, D. M.; Dawe, L. N.; Boeré, R. T.; Bodwell, G. J. Gram-Scale Synthesis and Highly Regioselective Bromination of 1,1,9,9-Tetramethyl[9](2,11)teropyrenophane. *Angew. Chem., Int. Ed.* **2018**, *57*, 1707–1711. See also: (c) Unikela, K. S.; Merner, B. L.; Ghasemabadi, P. G.; Warford, C. C.; Qiu, C. S.; Dawe, L. N.; Zhao, Y.; Bodwell, G. J. The Development of Synthetic Routes to 1,1,*n*-Tetramethyl[*n*](2,11)teropyrenophanes. *Eur. J. Org. Chem.* **2019**, 2019, 4546–4560. (d) Merner, B. L.; Unikela, K. S.; Dawe, L. N.; Thompson, D. W.; Bodwell, G. J. 1,1,*n*-Tetramethyl[*n*](2,11)-teropyrenophanes (*n* = 7–9) a Series of Armchair SWCNT Segments. *Chem. Commun.* **2013**, *49*, 5930–5932. (e) Merner, B. L.; Dawe, L. N.; Bodwell, G. J. 1,1,8,8-Tetramethyl[8](2,11)teropyrenophane: Half of an Aromatic Belt and a Segment of an (8,8)Single-Walled Carbon Nanotube. *Angew. Chem., Int. Ed.* **2009**, *48*, 5487–5491.
- (9) Bodwell, G. J.; Fleming, J. J.; Miller, D. O. Non-Planar Aromatic Compounds. 4. Fine Tuning the Degree of Bend in the Pyrene Unit of [7](2,7)Pyrenophanes by Modifying the Nature of the Bridge. *Tetrahedron* **2001**, *57*, 3577–3585.
- (10) Bodwell, G. J.; Bridson, J. N.; Cyrański, M.; Kennedy, J. W. J.; Krygowski, T. M.; Mannion, M. R.; Miller, D. O. Nonplanar aromatic Compounds. 8. Synthesis, Structure and HOMA Investigation of 1,*n*-Dioxa[*n*](2,7)pyrenophanes. How Does Bending Affect the Cyclic Pi Electron Delocalization of the Pyrene Unit? *J. Org. Chem.* **2003**, *68*, 2089–2098.
- (11) (a) Yang, Y.; Mannion, M. R.; Dawe, L. N.; Kraml, C. M.; Pascal, Jr. R. A.; Bodwell, G. J. A Synthetic Approach to [*n*](1,6)Pyrenophanes - Inherently Chiral [*n*]Cyclophanes. *J. Org. Chem.* **2012**, *77*, 57–67. For a less strained [*n*](1,6)pyrenophane, see: Mannancherry, R.; Devereux, M.; Häussinger, D.; Mayor, M. Molecular Ansa-Basket: Synthesis of Inherently Chiral All-Carbon [12](1,6)Pyrenophane. *J. Org. Chem.* **2019**, *84*, 5271–5276.
- (12) Nandaluru, P. R.; Dongare, P.; Kraml, C. M.; Pascal, R. A., Jr.; Dawe, L. N.; Thompson, D. W.; Bodwell, G. J. Concise, Aromatization-Based Synthesis of an Elaborate C₂-Symmetric Pyrenophane. *Chem. Commun.* **2012**, *48*, 7747–7749.
- (13) Pascal, R. A., Jr. Twisted Acenes. *Chem. Rev.* **2006**, *106*, 4809–4819.
- (14) Bodwell, G. J.; Bridson, J. N.; Houghton, T. J.; Kennedy, J. W. J.; Mannion, M. R. 1,7-Dioxa[7](2,7)pyrenophane: The Pyrene Unit is More Bent Than That of C₇₀. *Chem. - Eur. J.* **1999**, *5*, 1823–1827.
- (15) Biswas, S.; Qiu, C. S.; Dawe, L. N.; Zhao, Y.; Bodwell, G. J. Contractive Annulation: A Strategy for the Synthesis of Small, Strained Cyclophanes and its Application in the Synthesis of [2](6,1)Naphthaleno[1]paracyclophane. *Angew. Chem., Int. Ed.* **2019**, *58*, 9166–9170.
- (16) (a) Winnik, F. M. Photophysics of Preassociated Pyrenes in Aqueous Polymer Solutions and Other Organized Media. *Chem. Rev.* **1993**, *93*, 587–614. (b) Birks, J. B. *Photophysics of Aromatic Molecules*; Wiley-Interscience: London, 1970.
- (17) Maeda, H.; Akai, T.; Segi, M. Photo-Fries Rearrangement of 1-Pyrenyl Esters. *Tetrahedron Lett.* **2017**, *58*, 4377–4380.
- (18) Zych, D. Non-*K*-Region Disubstituted Pyrenes (1,3-, 1,6-, and 1,8-) by (Hetero)Aryl Groups-Review. *Molecules* **2019**, *24*, 2551–2583 and references therein.
- (19) Bodwell, G. J.; Nandaluru, P. R. Olefination Reactions in the Synthesis of Cyclophanes. *Isr. J. Chem.* **2012**, *52*, 105–138.
- (20) Williams, A. T. R.; Winfield, S. A.; Miller, J. N. Relative Fluorescence Quantum Yields Using a Computer-controlled Luminescence Spectrometer. *Analyst* **1983**, *108*, 1067–1071.
- (21) Bodwell, G. J.; Ernst, L.; Haelen, M.; Hopf, H. *Syn- and Anti-[2.2]Orthometacyclophane*. *Angew. Chem.* **1989**, *101*, 509–510.
- (22) (a) Zhao, Y.; Truhlar, D. G. The M06 Suite of Density Functional for Main Group Thermochemistry, Thermochemical Kinetics, Noncovalent Interactions, Excited States, and Transition Elements: Two new Functionals and Systematic Testing of Four M06-Class Functionals and 12 Other Functionals. *Theor. Chem. Acc.* **2008**, *120*, 215–241. (b) Mardirossian, N.; Head-Gordon, M. How Accurate are the Minnesota Density Functionals for Noncovalent Interactions, Isomerization Energies, Thermochemistry, and Barrier Heights Involving Molecules Composed of Main-Group Elements? *J. Chem. Theory Comput.* **2016**, *12*, 4303–4325. (c) Leang, S. S.; Zahariev, F.; Gordon, M. S. Benchmarking the Performance of Time-Dependent Density Functional Methods. *J. Chem. Phys.* **2012**, *136*, 104101. Jacquemin, D.; Perpète, E. A.; Ciofini, I.; Adamo, C.; Valero, R.; Zhao, Y.; Truhlar, D. G. On the Performances of the M06 Family of Density Functionals for Electronic Excitation Energies. *J. Chem. Theory Comput.* **2010**, *6*, 2071–2085.